Clays and Clay Minerals, Vol. 49, No. 2, 109–118, 2001.

TRANSMISSION ELECTRON MICROSCOPY STUDY OF CONVERSION OF SMECTITE TO ILLITE IN MUDSTONES OF THE NANKAI TROUGH: CONTRAST WITH COEVAL BENTONITES

HARUE MASUDA,[1] DONALD R. PEACOR,[2] AND HAILIANG DONG[2]†

[1]Department of Geosciences, Osaka City University, Sumiyoshi, Osaka 558-8585 Japan
[2]Department of Geological Sciences, The University of Michigan, Ann Arbor, Michigan 48109, USA

Abstract—Clay minerals in shales from cores at Site 808, Nankai Trough, have been studied using X-ray diffraction (XRD), scanning transmission electron microscopy (STEM), and analytical electron microscopy (AEM) to compare the rates and mechanisms of illitization with those of coeval bentonites, which were described previously. Authigenic K-rich smectite having a high Fe content (~7 wt. %) was observed to form directly as an alteration product of volcanic glass at a depth of ~500 meters below seafloor (mbsf) with no intermediate precursor. Smectite is then largely replaced by Reichweite, R, (R = 1) illite-smectite (I–S) and minor illite and chlorite over depths from ~550 to ~700 mbsf. No further mineralogical changes occur to the maximum depth cored, ~1300 m. Most smectite and I–S in shales are derived from alteration of glass, rather than being detrital, as is usually assumed. Discrete layer sequences of smectite, I–S, or illite coexist, indicating discontinuities of the transformation from smectite to (R = 1) I–S to illite. Authigenic Fe-rich chlorite forms concomitantly with I–S and illite, with the source of Fe from reactant smectite.

Smectite forms from glass with an intermediate precursor in coeval bentonites at approximately the same depth as in shales, but the smectite remains largely unchanged, with the exception of exchange of interlayer cations (K → Na → Ca) in response to formation of zeolites, to the bottom of the core. Differences in rates of illitization reflect the metastability of the clays. Temperature, structure-state, and composition of reactant smectite are ruled out as determining factors that increase reaction rates here, whereas differences in water/rock ratio (porosity/permeability), Si and K activities, and organic acid content are likely candidates.

Key Words—Bentonites, Diagenesis, Illite, Marine Sediments, Mixed-Layered I–S, Nankai Trough, Shales.

INTRODUCTION

Despite many studies and voluminous literature relating to the mechanism of the transformation of smectite to illite, there remains significant disagreement about the mineralogical characteristics of smectite, transitional illite-smectite (I–S) and illite, and the process of transformation. The lack of agreement about the structure of such phases mostly concerns the degree to which layer sequences are regarded as coherent or turbostratically stacked, *i.e.*, whether sequences are imperfect three-dimensional crystals or collections of fundamental particles (*e.g.*, Dong *et al.*, 1997; Guthrie and Reynolds, 1998; Nadeau, 1998; Peacor, 1998). Contrasting models of the process of transformation were reviewed by Altaner and Ylagan (1997, and references therein); models vary from layer-by-layer replacement to dissolution/transport/precipitation. There are also contrasting conclusions regarding the prograde sequence of phases. For example, Drits *et al.* (1997) proposed a continuous series of interstratified I–S, whereas Dong *et al.* (1997) emphasized the dominance of discrete smectite, (R = 1 where R = Reichweite) I–S, and illite.

Because the sequence from smectite through illite occurs in many different locations as a simple function of depth and therefore of increasing temperature (*e.g.*, Hower *et al.*, 1976), many have attempted to relate I–S to temperature of formation (*e.g.*, Eslinger and Glasmann, 1993). The sequences of phases from smectite to illite involve metastable clays, which react following the Ostwald step rule (*e.g.*, Essene and Peacor, 1995). The rate of transformation may therefore be affected by many variables, including temperature, fluid/rock ratio, and fluid composition (Small, 1993; Velde and Vasseur, 1992; Aja *et al.*, 1991; Huang *et al.*, 1993; Abercrombie *et al.*, 1994), *i.e.*, by any variable affecting reaction rate which promotes reaction of a metastable system toward the stable system.

The controversies regarding the coherency of layer sequences of smectite, I–S, and illite, and the processes of transformation, have been inferred, at least partly, from different rock types (*e.g.*, shales, bentonites, hydrothermal systems). Thus, these observations may be all valid with differences being a function of the different paths taken by reactions involving metastable phases under different conditions (*e.g.*, Li *et al.*, 1997). One way to resolve those differences is to study clay sequences subjected to nearly identical conditions, but in diverse rock types.

†Present address: Department of Geology, Miami University, Oxford, Ohio 45056, USA.

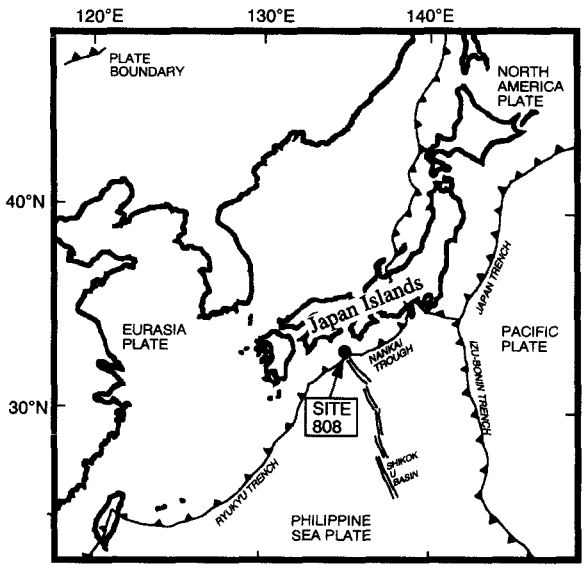

Figure 1. Location of ODP Site 808 in the Nankai Trough, within an accretionary wedge.

Sharply defined contrasts in the rate of conversion of smectite to illite occur between coeval bentonites and fine-grained clastic rocks, including shale. Many authors have demonstrated that in a given sediment sequence where different rock types occur, illite consistently develops more rapidly and at shallower depths in shales than in bentonites (*e.g.,* Merriman *et al.,* 1995; Li *et al.,* 1997). Sediments of the Nankai Trough are such an example, being an unusually well-defined sequence of smectite to illite where the degree of conversion is more advanced in shales than in bentonites. Masuda *et al.* (1993, 1996) used transmission electron microscopy (TEM) and X-ray diffraction (XRD) to detail the changes in mineral assemblages in bentonite in core samples in an accretionary wedge at ODP site 808 in the Nankai Trough. Volcanic glass in shallow samples was altered progressively to an intermediate layered material that was a precursor to smectite, and subsequently to smectite and zeolites. STEM (scanning transmission electron microscopy), TEM, SEM (scanning electron microscopy), and XRD data failed to show subsequent conversion of smectite to illite. In sharp contrast, however, conversion of smectite to I–S was reported in the interbedded shales (Underwood *et al.,* 1993). Thus, the differences in physico-chemical characteristics of authigenic mineralogy and original sediments in the same sediment column may provide evidence of those variables that affect the rate of formation of illite during early diagenesis.

The Nankai Trough is an ideal system to contrast the features of clay transitions in bentonites and shale because: (1) samples represent different degrees of transition in coeval shales and bentonites, (2) sediments were continuously sampled over a single core representing changing conditions, (3) fluids were sampled and studied, (4) transitions are now occurring as indicated by Ar/Ar dating of the <2-μm size fraction (Dong *et al.,* 1998) and therefore the samples were unaffected by subsequent geologic events, and (5) the bentonites were studied previously. We therefore studied the shales from ODP Site 808 using XRD, TEM, and analytical electron microscopy (AEM) for comparison with data for the coeval bentonites.

GEOLOGIC SETTING AND SAMPLES

The Nankai Trough is the locus of an active plate boundary where the Philippine Sea plate is being subducted beneath the Eurasian plate (Figure 1). Thick sediments filling the trench of the Nankai Trough comprise one of the best-documented modern accretionary prisms. Drilling at site 808 during ODP Leg 131 resulted in 1300 m of sediment core that intersected the décollement zone at 940–950 meters below sea floor (mbsf), terminating in basement basalt. The column is divided into two types of sediment separated by 50 m of transitional sediment; the upper 600 m is turbiditic trench fill and the lower is pelagic sediment (Shipboard Scientific Party, 1991). The temperature gradient of the column is high (10°C/100 m), owing to expulsion of hot fluids from the décollement zone (Shipboard Scientific Party, 1991).

XRD data (Underwood *et al.,* 1993) for shales showed that smectite occurred in the shallow samples, with an illite component in I–S first detected at 500 mbsf corresponding to 20% I in (R = 0) I–S at a temperature of 50°C. This temperature corresponds to the depth of the uppermost part of the transition zone from the shallower turbiditic to the deeper pelagic sediments. The XRD data imply that the proportion of illite layers increases with increasing depth. By contrast, no illite was recognized in the interstratified bentonite layers, as determined both by TEM and XRD (Masuda *et al.,* 1996) in the entire core. Clinoptilolite was detected at 600 mbsf (~60°C), at which depth the K of smectite, which was the dominant interlayer cation at shallower depths, was replaced by Na.

Samples were initially identified as shales (or mudstones) from hand-specimen appearance, in part by the black color which is probably caused by organic material. Bulk samples and <2-μm size fractions were analyzed by XRD to verify that they were representative of the sequence of mineral assemblages as defined by Masuda *et al.* (1993, 1996) and Underwood *et al.* (1993), and to obtain TEM samples representing the transformation sequence. The samples were produced by squeezing out pore water. These fluids were chemically analyzed (Shipboard Scientific Party, 1991). Because clinoptilolite and analcime were known to be alteration products of volcanic glass in the bentonites, shales containing zeolites were

excluded to provide as great a contrast as possible with the previously studied bentonites. Five samples were selected for TEM and AEM analysis.

EXPERIMENTAL METHODS

In addition to XRD patterns of bulk materials, air-dried and ethylene-glycol saturated <0.1-μm size fractions were analyzed by XRD using Ni-filtered CuKα radiation (10 mA, 30 kV) to determine the authigenic clay-mineral assemblages.

Small blocks of air-dried samples were impregnated (Kim *et al.*, 1995) with L. R. White resin to prevent collapse of hydrated interlayers in either the vacuum of the ion mill or TEM. The procedure allows smectite, illite, or (R = 1) I–S layers, each with characteristic spacings, to be identified. Thin sections were prepared to thicknesses of <10 μm, and ion milled to <0.1 μm. TEM observations were made using a Philips CM12 instrument with a Kevex Quantum EDS system for chemical analysis. AEM data were analyzed following Ahn and Peacor (1988). Errors in quantitative mineral analysis are believed to be <5 wt. %.

Illite, I–S, and smectite were tentatively identified in TEM images by characteristic layer spacings and contrast (see Dong *et al.*, 1997). Packets of illite layers tend to have straight, parallel layers with constant contrast; smectite has anastomosing layers with variable contrast, common layer terminations, and ill-defined boundaries; and I–S has intermediate characteristics. Identification was based collectively from these characteristics, selected area electron diffraction (SAED) patterns, and AEM analyses.

RESULTS

XRD data

XRD patterns of bulk samples showed that the shales are composed of approximately the same proportions of major minerals at all depths. The samples contain ~50% quartz, 25% feldspar, and 20% total clay minerals (muscovite and/or illite, chlorite, and smectite or I–S), with minor calcite, hornblende, and heulandite or clinoptilolite. Quartz, feldspar, muscovite, and chlorite were inferred to be largely detrital in origin because the concentrations were similar at all depths. The proportion of authigenic clay is therefore relatively small. In contrast, mineral assemblages of bentonites have a high authigenic clay proportion. Although smectite is present at all depths, implying that some is of detrital origin, the proportion is relatively constant until ~500 mbsf, at which depth the proportion of smectite increases, followed by a decrease at ~800 mbsf. The decrease in smectite is accompanied by an increase in chlorite (Underwood *et al.*, 1993). These changes correlate with an increase in the relative proportion of bentonite layers interbedded with the shales.

Selected XRD patterns of <0.1-μm size fractions of shales are shown in Figure 2. The dominant phase is smectite with $d(001)$ of ~14.7 Å in air-dried samples, and 17 Å in ethylene glycol-solvated samples. Although the peak is weak, the d value of (060) is 1.50 Å for air-dried samples, implying that the smectite is dioctahedral. A peak with d of ~8.8 Å was observed for all ethylene glycol-treated samples obtained from depths of >685 mbsf, indicating (R = 1) I–S (Reynolds, 1992; Moore and Reynolds, 1997). The position of this peak did not change with increasing depth, implying a constant proportion of illite in I–S.

STEM observations

At 512 mbsf (~50°C). Three types of phases are present: (1) detrital minerals, (2) volcanic glass, and (3) smectite. The dominant detrital minerals are quartz, hornblende, feldspars, muscovite, and chlorite. TEM images of these grains are similar at all depths and show that these minerals are commonly in the micrometer-size range. They have angular outlines as typical of detrital minerals unmodified by diagenesis.

Volcanic glass was identified by its lack of SAED pattern and contrast in TEM images, and its textural relation to smectite to which it alters. Figure 3 shows a rounded grain of glass, with layers of smectite wrapped around and parallel to the surface, and with no discernible sharp boundary between smectite and the glass. Smectite shows the texture typical of alteration from glass. It occurs as anastomosing layers of thin packets which often appear to enclose space. There is no preferred orientation parallel to bedding. Similar textures were interpreted as direct alteration of glass to smectite (Eggleton, 1987; Tazaki *et al.*, 1989; Masuda *et al.*, 1996). This curvature, especially where layers curve in doughnut-shaped units, is inferred to be an inheritance of the shape of glass shards (Figure 3) where the transformation from glass is incomplete.

At 685 mbsf (~70°C). The clays range from smectite to illite. Thin packets of illite layers occur embedded within a matrix of continuous layers of either I–S or smectite (Figure 4). The texture of this and deeper samples contrasts markedly with the shallower samples, in that the cell-like texture typical of smectite is present only locally, having been replaced by smectite and I–S layers that are subparallel to one another and to bedding.

At 907 mbsf (~90°C). Figure 5 shows smectite and I–S. The layers are straight and subparallel (presumably to bedding) compared to those at shallow depths. Figure 5 shows a packet of illite of ~15 layers thick within a matrix of subparallel, anastomosing layers of I–S. Layer contrast and spacings imply that the I–S is dominantly (R = 1) I–S, but with disorder in the layer sequence; *e.g.*, ISI and ISII units are common and

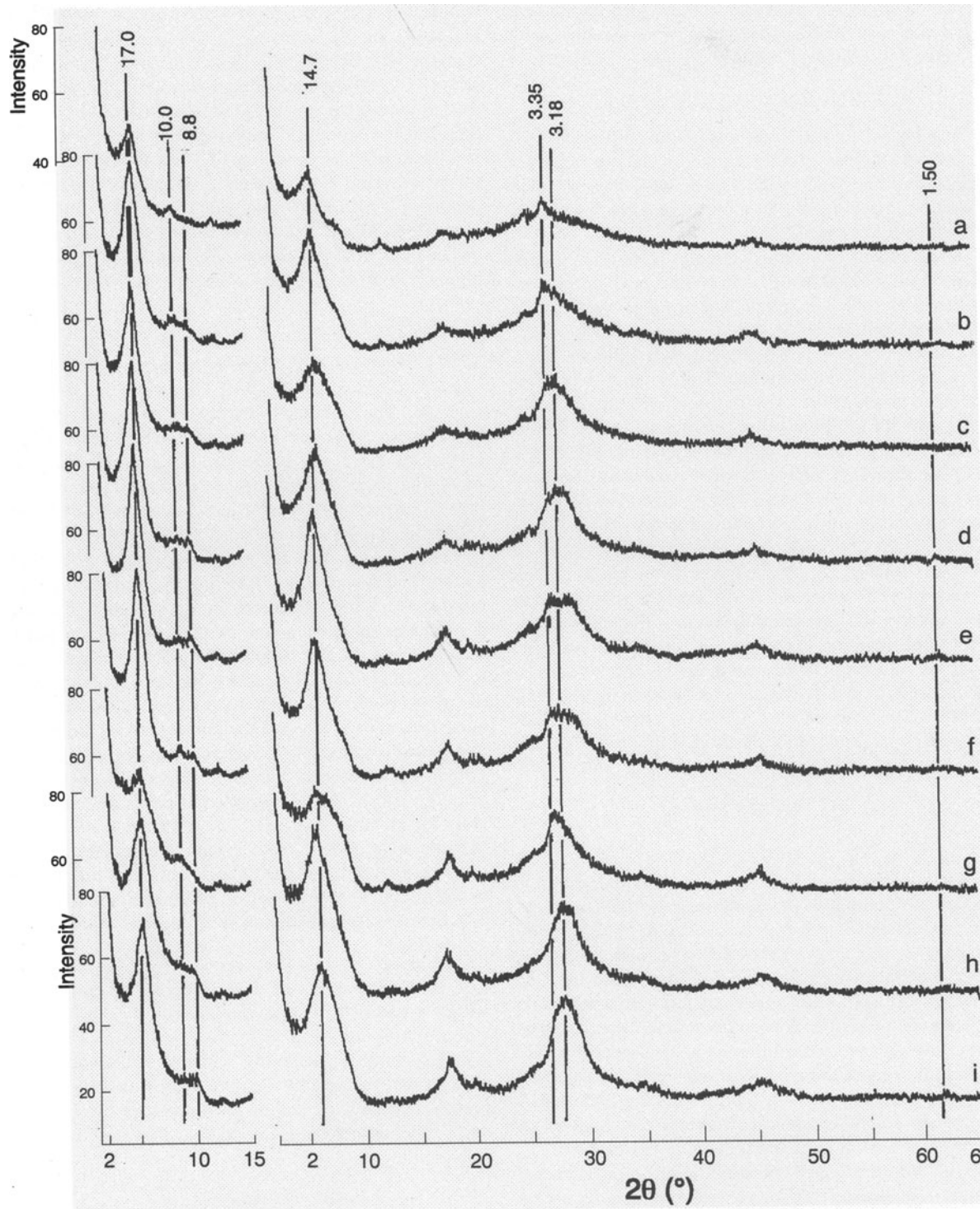

Figure 2. X-ray diffraction patterns of <0.1-μm size fractions of shales from ODP Site 808 in the Nankai Trough. Samples labeled TEM were used in TEM studies. Depths of samples (mbsf: meters below seafloor) are as follows: (a) 512; TEM, (b) 578, (c) 685; TEM, (d) 822, (e) 852, (f) 907; TEM, (g) 909, (h) 1147; TEM, and (i) 1176; TEM.

https://doi.org/10.1346/CCMN.2001.0490201 Published online by Cambridge University Press

Figure 3. TEM lattice-fringe image of smectite from 512 mbsf. Curved packets commonly form circular units (inferred to be spherical in three dimensions) that result from progressive alteration toward the core of glass shards, with smectite layers wrapping around shards (not shown).

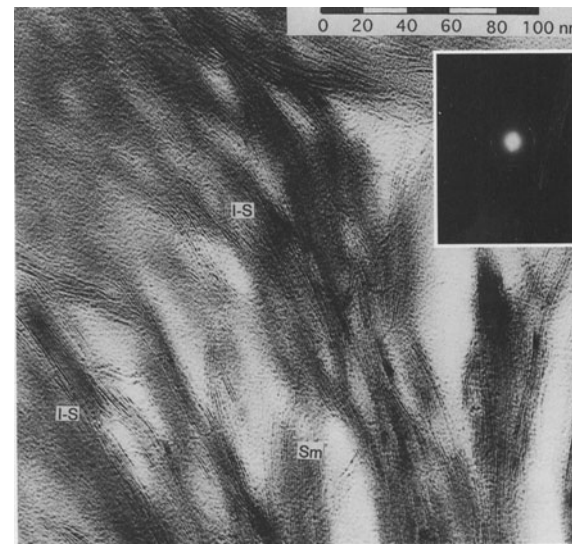

Figure 5. TEM lattice-fringe image of shale from 907 mbsf. Arrays of subparallel layers consisting largely of I–S, with abundant pore space representing original sediment porosity. The abbreviations are as follows; Sm: smectite; I–S: illite-smectite interstratified clay minerals.

occur randomly and the proportion of illite-like layers is >50%.

At 1147 and 1176 mbsf (~115 to 120°C). These two samples are nearly identical in mineral assemblage and texture, and closely resemble those from 685 and 907 mbsf. These samples contain continuous sequences of anastomosing layers of smectite and I–S (Figures 7 and 8a). Authigenic chlorite is inferred to be a by-product of illitization of smectite (Figure 8b) (see below). As shown in Figures 7 and 8a, subparallel layers are discontinuous with frequent layer terminations, with marked curvature. They form a near continuous array similar to the "megacrystals" in Gulf Coast shales (Ahn and Peacor, 1985). Nevertheless, layer sequences consist either of smectite or (R = 1) I–S (Figure 9). Illite and chlorite occur in separate packets of ≥10 layers within the I–S or S matrix.

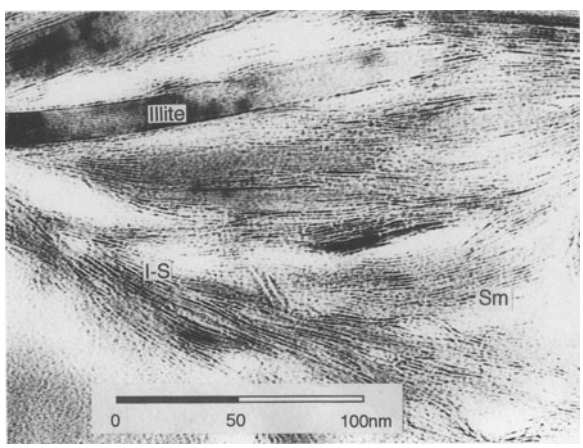

Figure 4. TEM lattice-fringe image of shale from 685 mbsf. A packet of illite of ~150 Å thick is subparallel to thin packets of (R = 1) I–S, with fringes of I–S showing weak alternating darker and lighter contrast. Sequences of smectite layers occur locally. The abbreviations are as follows; Sm: smectite; I–S: illite-smectite interstratified clay minerals.

Chemical composition of clay minerals

Typical chemical compositions of authigenic smectite, illite, chlorite, and I–S analyzed by AEM are shown in Table 1. As described above, no packets of homogeneous authigenic clay minerals occur at the scale of resolution of AEM analysis and thus the anal-

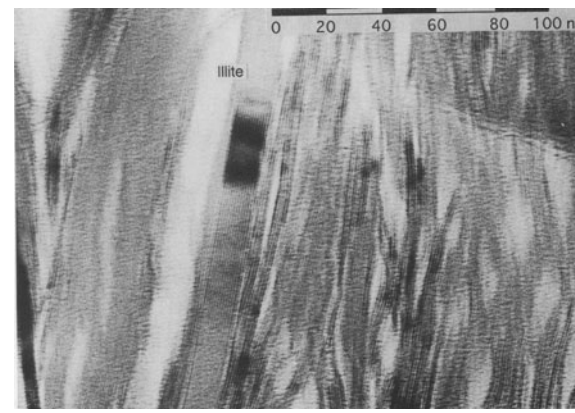

Figure 6. TEM lattice-fringe image of shale from 907 mbsf. A thin packet of illite is subparallel to thin packets of I–S.

https://doi.org/10.1346/CCMN.2001.0490201 Published online by Cambridge University Press

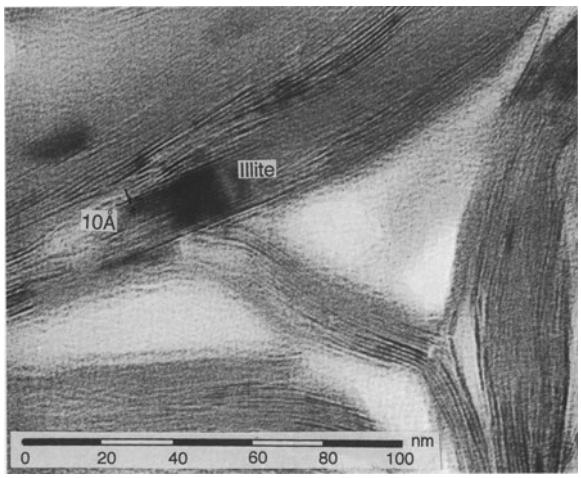

Figure 7. TEM lattice-fringe image of shale from 1176 mbsf. A short, thick sequence of illite layers is embedded within a sequence of I–S. Abundant pore space is defined largely by high-angle intersections of packets of I–S.

yses may be contaminated by other phases. Nevertheless, the average compositions are in agreement with single-phase clay minerals.

Smectite. Although the proportions of Al, Fe, and Mg vary widely within the same TEM sample, the average composition approximates Fe- and Mg-rich montmorillonite. Similar compositions were observed by Masuda *et al.* (1996) for smectite derived by alteration of volcanic glass in bentonites coeval with the shales, implying a similar origin for both. As is commonly observed for authigenic smectite originating in marine sediments, K is usually the dominant interlayer cation.

There are trends of increasing Si, and decreasing ^{IV}Al, Fe, and Mg with increasing depth. The average K content of all samples, except the sample from 512 mbsf, is weakly decreasing with increasing depth. These samples contain similar proportions of S, I–S, and illite, and reflect a constant mineral assemblage. The small decrease in K content of smectite is inferred to result from utilization of K in illitization, as discussed below.

Illite. The compositions are notable in being relatively constant as a function of depth, as expected for authigenic illite of common origin and with a single layer type. Compared with smectite, authigenic illite is enriched in K and depleted in Fe. Although such trends are common for illitization, the relatively high Si contents and low interlayer-cation contents compared to ideal illite imply inclusion of smectite in the areas analyzed. Thus, only general trends in composition are interpreted as significant.

I–S. I–S is intergrown with smectite-like and illite-like layer sequences which cannot be resolved. Thus, only average compositions of I–S from two depths (907 and

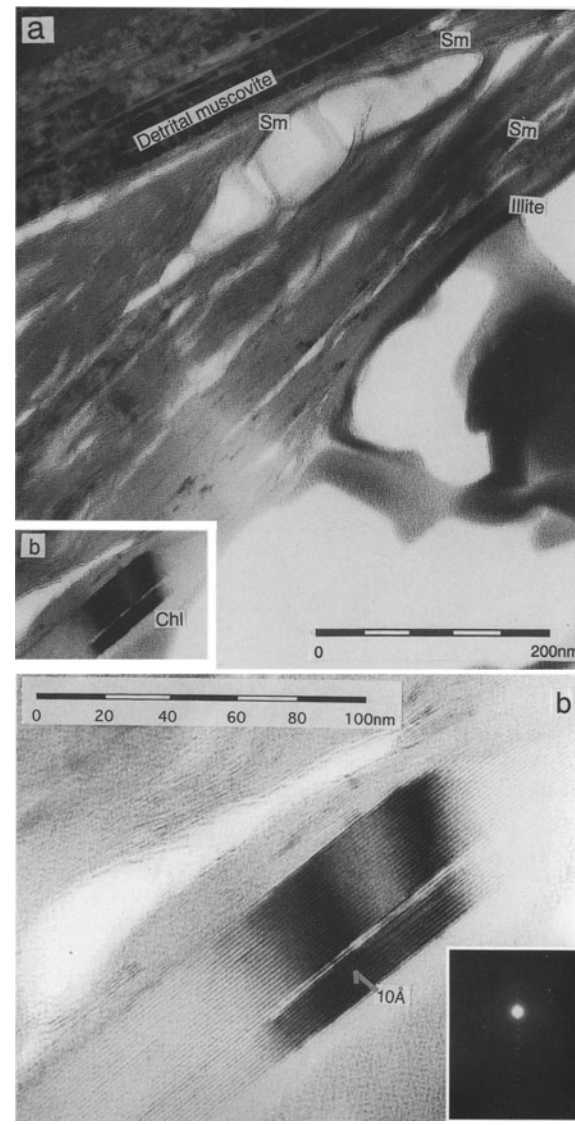

Figure 8. (a) Lattice-fringe image of shale from 1176 mbsf showing a large grain of detrital muscovite bordered by packets of authigenic smectite, illite and chlorite. (b) Enlargement of boxed area of Figure 8a, showing a thin chlorite packet having 7-Å fringes with a single 10-Å fringe (indicated by an arrow) as typical of authigenic chlorite. The abbreviations are as follows; Sm: smectite; Chl: chlorite.

1176 m) approximate pure I–S. Compared with illite described above, I–S has greater proportions of Na and Ca.

Chlorite. Only one analysis of relatively pure authigenic chlorite was obtained owing to small packet sizes, but analyses of detrital chlorite were obtained. Both detrital and authigenic chlorites are unusual in having high Fe contents, and may be classified as chamosite rather than clinochlore, which is more typical of authigenic chlorite in pelites.

https://doi.org/10.1346/CCMN.2001.0490201 Published online by Cambridge University Press

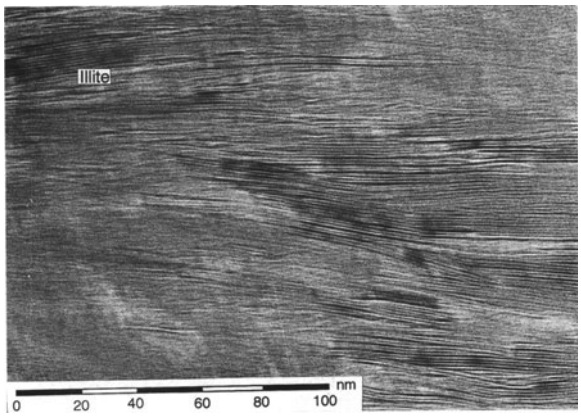

Figure 9. TEM lattice-fringe image of shale from 1176 mbsf showing the typical continuous arrays which are dominantly comprised of I–S, but with thin sequences of illite layers occurring locally. The abbreviation is as follows; I–S: illite-smectite interstratified clay minerals.

DISCUSSION

Discontinuities in the down-core smectite-to-illite sequence in shale

XRD data of Underwood *et al.* (1993) showed that the proportion of minerals in bulk samples is nearly constant over the >1300 m of core, corresponding to quartz (~50%), plagioclase (<30%), clay minerals (20%), and calcite (<5%). XRD data for the <2-μm size fraction showed that the proportion of smectite is approximately constant from the surface to >500 mbsf. Smectite increases at 500–600 mbsf, maximizes at ~800 mbsf, and decreases at greater depths. XRD data were obtained here for samples at >500 mbsf, to verify the data of Underwood *et al.* (1993).

The sample from 512 mbsf was therefore chosen for TEM studies to be representative of the beginning of the S → I transition interval. TEM images show residual glass in the process of direct alteration to smectite. The smectite, in curved packets wrapped around glass, or with equivalent textures, and XRD data collectively imply that most smectite in shallower samples is detrital, and that smectite from greater depths is both detrital and authigenic. Masuda *et al.* (1996) concluded that significant alteration of volcanic glass to smectite in bentonites was first detected at depths near 670 mbsf. This is ~100 m deeper than the equivalent depth in shales, but qualitatively comparable. In samples from ~800 mbsf, the smectite of shales would dominantly be derived from direct alteration of volcanic glass. We suggest that in other instances where smectite-bearing shales are composed of minerals derived through terrigenous alteration, an origin of smectite in part owing to alteration of volcanic glass during

Table 1. Average major element composition of authigenic clay minerals and detrital chlorite in shales from ODP Site 808, Nankai Trough.

Mineral depths (mbsf)	Sm 512	(1σ)	Sm 685	(1σ)	Sm 907	(1σ)	Sm 1146	(1σ)	Il 685	Il 907	Il 1176	[1]Chl 1176	[2,3]Chl 1176	I-S 907	I-S 1176
SiO_2 (%)	55.0	2.8	56.4	0.3	57.7	2.7	60.7	3.7	57.9	57.7	58.3	30.3	33.9	57.2	58.8
TiO	0.5	1.3	0.5	0.7	0.0		0.4	0.8	0.0	0.0	0.5	0.0	0.0	0.15	0
Al_2O_3	22.1	4.7	22.1	3.2	22.0	3.2	22.9	2.6	22.5	24.4	23.1	19.4	21.7	23.1	23.8
FeO*	8.5	3.7	7.8	3.5	7.6	2.1	4.6	0.6	6.0	3.2	6.0	39.6	31.9	5.8	5.0
MnO	0.1	0.3	0.1	0.2	0.1	0.3	0		0.0	0.0	0.4	0.9	1.4	0	0.2
Cr_2O_3	0.5	1.3	0.0		0.1	0.2	0		0.0	0.0	0.2	—	—	0	0.2
MgO	2.2	1.4	2.6	0.4	2.3	0.6	2.2	0.3	2.0	2.6	1.7	4.5	5.3	2.6	1.9
CaO	0.3	0.6	0.3	0.4	0.7	0.4	0.4	0.3	0.0	0.3	0.0	0	0.1	0.8	0.7
Na_2O	1.7	1.5	2.3	0.2	1.3	0.9	0.8	0.6	1.3	0.0	0.0	0	0.3	1.9	1.0
K_2O	4.1	0.8	3.0	0.2	3.3	1.2	3.1	1.2	5.2	4.3	5.0	0.4	0.3	3.5	3.5
Total	95.0		95.0		95.0		95.0		95.0	95.0	95.0	95.0	94.9	95.0	95.0
Numbers of ions calculated based on 20 O and 4 (OH)															
Si	7.32		7.41		7.54		7.73		7.58	7.55	7.58				
Ti	0.05		0.05		0		0.04		0.00	0.00	0.05				
Al (tet)	0.63		0.54		0.46		0.23		0.42	0.45	0.38				
Al (oct)	2.82		2.86		2.92		3.2		3.04	3.31	3.15				
Fe	0.95		0.86		0.83		0.49		0.66	0.35	0.65				
Mn	0.01		0.01		0.02		0		0.00	0.00	0.04				
Cr	0.06		0		0.01		0		0.00	0.00	0.02				
Mg	0.43		0.51		0.45		0.42		0.39	0.51	0.33				
Ca	0.04		0.04		0.1		0.05		0.00	0.04	0.00				
Na	0.42		0.59		0.33		0.19		0.34	0.00	0.00				
K	0.7		0.5		0.55		0.51		0.87	0.73	0.83				

[1] Authigenic chlorite.
[2] Detrital chlorite.
[3] Chemical composition of detrital chlorite is an average of those from 512, 685, 907, and 1146 mbsf.
* All iron assumed as FeO.

https://doi.org/10.1346/CCMN.2001.0490201 Published online by Cambridge University Press

diagenesis, rather than as a detrital mineral, should be considered.

The XRD data (this study and Underwood *et al.,* 1993) showed that interstratified I–S is the dominant dioctahedral clay mineral at depths greater than ~650 mbsf. Underwood *et al.* (1993) reported that the illite content in I–S from the <2-μm size fraction increased with increasing depth, with 80% illite in I–S in the deepest shales. The XRD data here were obtained from the <0.1-μm fraction, and, in contrast, showed that the interstratified I–S displayed no detectable change with increasing depth. These differences are probably related to grain-size differences. The smaller size fraction more closely reflects the state of the authigenic grains as compared to larger detrital grains. TEM observations of samples from 685, 907, 1146, and 1176 mbsf are in agreement with the XRD data. The lattice-fringe images of dioctahedral clay minerals from each sample are dominated by (R = 1) I–S. Thus, these samples show sequences dominated by IS units, but with randomly dispersed ISI and ISII units, as well as rare units with larger numbers of illite-like interlayers.

Lattice-fringe images show that I–S is commonly associated with separate illite-rich packets. These illite packets also contain small sequences of smectite interlayers. I–S-rich samples are therefore comprised largely of (R = 1) I–S, and with separate smectite- and illite-rich packets. This observation is similar to that of Dong *et al.* (1997), who observed packets from Gulf Coast and other shales dominated by smectite, (R = 1) I–S (~50% I), or illite.

The collective data demonstrate that the authigenic dioctahedral clay of shales is derived through alteration of volcanic glass starting at ~500 mbsf, and is replaced primarily by (R = 1) I–S coexisting with minor smectite in shallower samples, and by (R = 1) I–S coexisting with illite and some smectite in deeper samples. The (R = 1) I–S remains relatively unchanged with increasing depth. There are thus two discontinuities in the sequence of clay minerals, one between smectite and (R = 1) I–S, and a limited gap between (R = 1) I–S and illite, as consistent with the data and conclusions of Dong *et al.* (1997) for sequences from other localities.

Authigenic chlorite

Packets of Fe-rich chlorite were observed in samples at >941 mbsf (Figure 8; Table 1). These packets are all probably authigenic as they are thin, similar in thickness to those of authigenic illite, and at least two orders of magnitude smaller than those of detrital origin. The smectite of shallower samples is unusually Fe-rich (Table 1). The authigenic I–S has a much smaller and more typical Fe content. Assuming that I–S is a replacement product of smectite, these data are consistent with the utilization of excess Fe in the formation of chlorite during illitization. Ahn and Peacor (1985) suggested a similar origin for some of the authigenic chlorite in Gulf Coast mudstones.

Interlayer composition of smectite

Direct chemical analyses of smectite in marine sediments have shown that K is usually the dominant interlayer cation (Hover and Peacor, 1999), as in this study, including smectite altering from volcanic glass. As shown by Masuda *et al.* (1996), the composition of smectite that is altering from volcanic glass is closely related to that of the glass. The glass has K ≫ Na, Ca and this implies that such K is a probable source of interlayer K in smectite. The K of marine waters, either near-surface or pore water in the sediment column, may also be a source of K. The data presented here provide another example of the K-rich nature of much, if not most, smectite in marine sediments.

Comparison of illitization rates in coeval bentonites and shales

The data of this study confirm that the rates of illitization in the coeval bentonites and shales of the Nankai Trough are different. Although authigenic smectite forms from volcanic glass at approximately the same depth, the smectite of bentonite remains unchanged at greater depth, except for interlayer cation composition. Over a 100–200-m depth range, however, smectite of shales is replaced by I–S (~50% I), which subsequently remains nearly unchanged with greater depth to the bottom of the core, ~1300 mbsf. As noted above, where the rate of illitization differs between coeval bentonites and shales, the process lags behind in bentonites (*e.g.,* Altaner and Grim, 1990; Li *et al.,* 1998), as in the Nankai Trough.

The data of this study do not permit identification of the specific cause of varying reaction rates, but do present some insights as to possible causes. Several authors (*e.g.,* Essene and Peacor, 1995) showed that smectite, I–S, and illite are metastable phases relative to muscovite, and that the reactions between such phases are path-dependent; *i.e.,* reaction rates vary if the starting reactant is of different composition or structure. Smectite of bentonites is derived through alteration of volcanic glass, and progresses through a disordered phase which is a precursor to smectite, whereas the smectite of coeval shales is in part of detrital origin. For the shales of this study, however, most of the smectite is derived through alteration of volcanic glass at approximately the same depths as for bentonites. The differences in reaction rates must therefore be related to other causes.

Because the reactants and products are metastable, many variables may affect reaction rates, among which temperature, water/rock ratio, and fluid composition are especially significant. Temperature differ-

https://doi.org/10.1346/CCMN.2001.0490201 Published online by Cambridge University Press

ences are clearly not a determining factor in this case, because bentonites and shales are interbedded and are probably equally affected by temperature. High water/rock ratio has been emphasized to promote illitization (*e.g.,* Boles and Franks, 1979; Yau *et al.,* 1987; Ahn *et al.,* 1988; Whitney, 1990). We have no quantitative data on differences in water/rock ratio in shales *versus* bentonites. SEM and TEM images do show that the textures of the two rock types are very different, bentonites having a continuous interlocking array of clay particles whereas shales are dominated by coarse grains of clastic sediments. Freed and Peacor (1989) emphasized that clay fabric affects porosity, and therefore permeability. Also, they showed that illitization causes a decrease in pore space, which may seal sediments and cause geopressuring. Greater porosity in the more coarsely grained shales will result in a greater water/rock ratio and will promote dissolution/neocrystallization, as is the case for shales *versus* sandstones.

Differences in fluid composition probably produced the different reaction rates (Huang *et al.,* 1993). Although fluids were sampled at the time of coring of the section studied herein, bentonite beds are thin, and fluid samples may be representative of large ranges in depth, therefore differences in fluid compositions between bentonites and shales could not be determined reliably. Nevertheless, K-rich clinoptilolite is common over a significant range of depths in the bentonite, and its presence depresses the rate of illitization (Altaner and Grim, 1989; Masuda *et al.,* 1996), by utilizing the K which is essential for the process. High activity of silica is required for crystallization of clinoptilolite relative to illite. Abercrombie *et al.* (1994) noted that the rate of illitization is controlled by silica activity, which in turn is controlled by the rate of precipitation of silica. I–S formation parallels that of maturation of organic material (*e.g.,* Lindgreen *et al.,* 1991). Small (1993) showed that the organic acids evolved during early diagenesis can be critical to rates of illitization, through their control on solubility of Al. Although the organic content of the shales and bentonites are unknown, white bentonites have little organic matter as opposed to black shales. The presence of organic matter in shales could therefore be the main factor in determining relative reaction rates.

ACKNOWLEDGMENTS

We thank A. Taira, the Shipboard Scientific Party, and crews of ODP Leg 131 for providing the studied samples. We are grateful for the constructive and helpful reviews of R.A. Eggleton and an anonymous reviewer. This work was supported by NSF grants EAR 94-18108 and 98-14391 to D.R. Peacor.

REFERENCES

Abercrombie, H.J., Hutcheon, I.E., Bloch, J.D., and deCaritat, P. (1994) Silica activity and the smectite-illite reaction. *Geology,* **22,** 539–542.

Ahn, J.H. and Peacor, D.R. (1985) Transmission electron microscopic study of diagenetic chlorite in Gulf Coast argillaceous sediments. *Clays and Clay Minerals,* **33,** 228–236.

Ahn, J.H. and Peacor, D.R. (1988) Transmission and analytical electron microscopy study of the smectite-to illite transition. *Clays and Clay Minerals,* **34,** 165–179.

Ahn, J.H., Peacor, D.R., and Coombs, D.S. (1988) Formation mechanisms of illite, chlorite and mixed-layer illite-chlorite in Triassic volcanogenic sediments from the Southland Syncline, New Zealand. *Contributions to Mineralogy and Petrology,* **99,** 82–89.

Aja, S.U., Rosenberg, P.E., and Kittrick, J.A. (1991) Illite equilibria in solution: I. Phase relationships in the system K_2O-Al_2O_3-SiO_2-H_2O between 25 and 250 °C. *Geochimica et Cosmochimica Acta,* **55,** 1353–1364.

Altaner, S.P. and Grim, R.E. (1990) Mineralogy, chemistry, and diagenesis of the tuffs in the Sucker Creek Formation (Miocene), eastern Oregon. *Clays and Clay Minerals,* **38,** 561–572.

Altaner, S.P. and Ylagan, R.F. (1997) Comparison of structural models of mixed-layer illite/smectite and reaction mechanisms of smectite illitization. *Clays and Clay Minerals,* **45,** 517–533.

Boles, J.R. and Franks S.G. (1979) Clay diagenesis in Wilcox sandstones of southwest Texas: Implications of smectite diagenesis on sandstone cementation. *Journal of Sedimentary Petrology,* **49,** 55–70.

Dong, H., Peacor, D.R., and Freed, R.L. (1997) Phase relations among smectite, R1 illite-smectite, and illite. *American Mineralogist,* **82,** 379–391.

Dong, H., Hall, C.M., Peacor, D.R., Masuda, H., and Halliday, A.M. (1998) $^{40}Ar/^{39}Ar$ dating of smectite formation in bentonites from Nankai Trough, Japan. *Clay Mineral Society Meeting Program and Abstracts, 34th Annual Meeting,* 76.

Drits, V., Środoń, J., and Eberl, D.D. (1997) XRD measurement of mean crystallite thickness of illite and illite/smectite: Reappraisal of the Kubler index and the Scherrer equation. *Clays and Clay Minerals,* **45,** 461–475.

Eggleton, R.A. (1987) Non-crystalline Fe-Si-Al-oxyhydroxides. *Clays and Clay Minerals,* **35,** 29–37.

Eslinger, E. and Glasmann, J.R. (1993) Geothermometry and geochronology using clay minerals—an introduction. *Clays and Clay Minerals,* **41,** 117–118.

Essene, E.J. and Peacor, D.R. (1995) Clay mineral thermometry—A critical perspective. *Clays and Clay Minerals,* **43,** 540–553.

Freed, R.L. and Peacor, D.R. (1989) Geopressured shale and sealing effect of the smectite to illite transition. *American Association of Petroleum Geologists Bulletin,* **73,** 1223–1232.

Guthrie, G. and Reynolds, R.C., Jr. (1998) A coherent TEM- and XRD-description of mixed-layer illite/smectite: Computer simulations. *Canadian Mineralogist,* **36,** 1421–1434.

Hover, V.C. and Peacor, D.R. (1999) Direct evidence for potassium uptake in smectite during early diagenesis of marine sediments and MORB: Balancing the global potassium budget. *Clay Mineral Society Meeting Program and Abstracts, 36th Annual Meeting,* Purdue University, West Lafayette, 50.

Hower, J., Eslinger, E.V., Hower, M.E., and Perry, E.A. (1976) Mechanism of burial metamorphism of argillaceous sediment: 1. Mineralogical and chemical evidence. *Geological Society of American Bulletin,* **87,** 725–737.

Huang, W.L., Longo, J.M., and Pevear, D.R. (1993) An experimentally derived kinetic model for smectite-illite conversion and its use as a geothermometer. *Clays and Clay Minerals,* **41,** 162–177.

Kim, J.-W., Peacor, D.R., Tessier, D., and Elsass, F.A. (1995) Technique for maintaining texture and permanent expansion of smectite interlayers for TEM observations. *Clays and Clay Minerals,* **43,** 51–57.

Li, G., Peacor, D.R., and Coombs, D.S. (1997) Transformation of smectite to illite in bentonite and associated sediments from Kaka Point, New Zealand: Contrast in rate and mechanism. *Clays and Clay Minerals,* **45,** 54–67.

Li, G., Peacor, D.R., and Essene, E.J. (1998) The formation of sulfides during alteration of biotite to chlorite-corrensite. *Clays and Clay Minerals,* **46,** 649–657.

Lindgreen, H., Jacobsen, H., and Jacobsen, H.J. (1991) Diagenetic structural transformations in North Sea Jurassic illite/smectite. *Clays and Clay Minerals,* **39,** 54–69.

Masuda, H., Tanaka, H., Gamo, T., Soh, W., and Taira, A. (1993) Major element chemistry and alteration mineralogy of volcanic ash, Site 808 in the Nankai Trough. In *Proceedings of Ocean Drilling Program Scientific Results 131B,* I. Hill, A. Taira, and J.V. Firth, eds., Ocean Drilling Program, College Station, Texas, 175–183.

Masuda, H., O'Neil, J.R., Jiang, W-.T., and Peacor, D.R. (1996) Relation between interlayer composition of authigenic smectite, mineral assemblages, I/S formation rate and fluid composition in silicic ash of the Nankai Trough. *Clays and Clay Minerals,* **44,** 443–459.

Merriman, R.J., Roberts, B., Peacor, D.R., and Hirons S.R. (1995) Strain-related differences in the crystal growth of white mica and chlorite: A TEM and XRD study of the development of metapelitic microfabrics in the Southern Uplands thrust terrane, Scotland. *Journal of Metamorphic Geology,* **13,** 559–576.

Moore, D.M. and Reynolds, R.C., Jr. (1997) *X-ray Diffraction and the Identification and Analysis of Clay Minerals, 2nd edition.* Oxford University Press, New York, 332 pp.

Nadeau, P.H. (1998) Evolution, current situation, and geological implications of the "fundamental particle" concept. *Canadian Mineralogist,* **36,** 1409–1414.

Peacor, D.R. (1998) Implications of TEM data for the concept of fundamental particles. *Canadian Mineralogist,* **36,** 1397–1408.

Reynolds, R.C., Jr. (1992) X-ray diffraction studies of illite/smectite from rocks, <1 μm randomly oriented powders, and <1 μm oriented powder aggregates: The absence of laboratory-induced artifacts. *Clays and Clay Minerals,* **40,** 387–396.

Shipboard Scientific Party (1991) Site 808. In I. Hill, A. Taira, and J.V. Firth, eds., *Proceedings of Ocean Drilling Program, Initial Reports, 131,* Ocean Drilling Program, College Station, Texas, 71–269.

Small, J.S. (1993) Experimental determination of the rates of precipitation of authigenic illite and kaolinite in the presence of aqueous oxalate and comparison to the K/Ar ages of authigenic illite in reservoir sandstones. *Clays and Clay Minerals,* **41,** 191–208.

Tazaki, K., Fyfe, W.S., and Van Der Gaast, S.J. (1989) Growth of clay minerals in natural and synthetic glasses. *Clays and Clay Minerals,* **37,** 348–354.

Underwood, M., Pickering, K., Gieskes, J.M., Kastner, M., and Orr, R. (1993) Sedimentary facies evolution of the Nankai forearc and its implications for the growth of the Shimanto accretionary prism. In *Proceedings of the Ocean Drilling Program, Scientific Results, 131B,* I. Hill, A. Taira, and J.V. Firth, eds., Ocean Drilling Program, College Station, Texas, 343–363.

Velde, B. and Vasseur, G. (1992) Estimation of the diagenetic smectite to illite transformation in time-temperature space. *American Mineralogist,* **77,** 967–976.

Whitney, G. (1990) Role of water in the smectite-to-illite reaction. *Clays and Clay Minerals,* **38,** 343–350.

Yau Y.-C., Peacor, D.R., and McDowell, S.D. (1987) Smectite-illite reactions in Salton Sea shales: A transition and analytical electron microscope study. *Journal of Sedimentary Petrology,* 57, 335–342.

E-mail of corresponding author: harue@sci.osaka-cu.ac.jp

(Received 27 November 1999; accepted 13 September 2000; Ms. 401; A.E. Stephen Altaner)